

Efficiency Second-Harmonic Propagation of Spin Waves in Thin Ferromagnetic Films with Out-of-Plane Magnetization

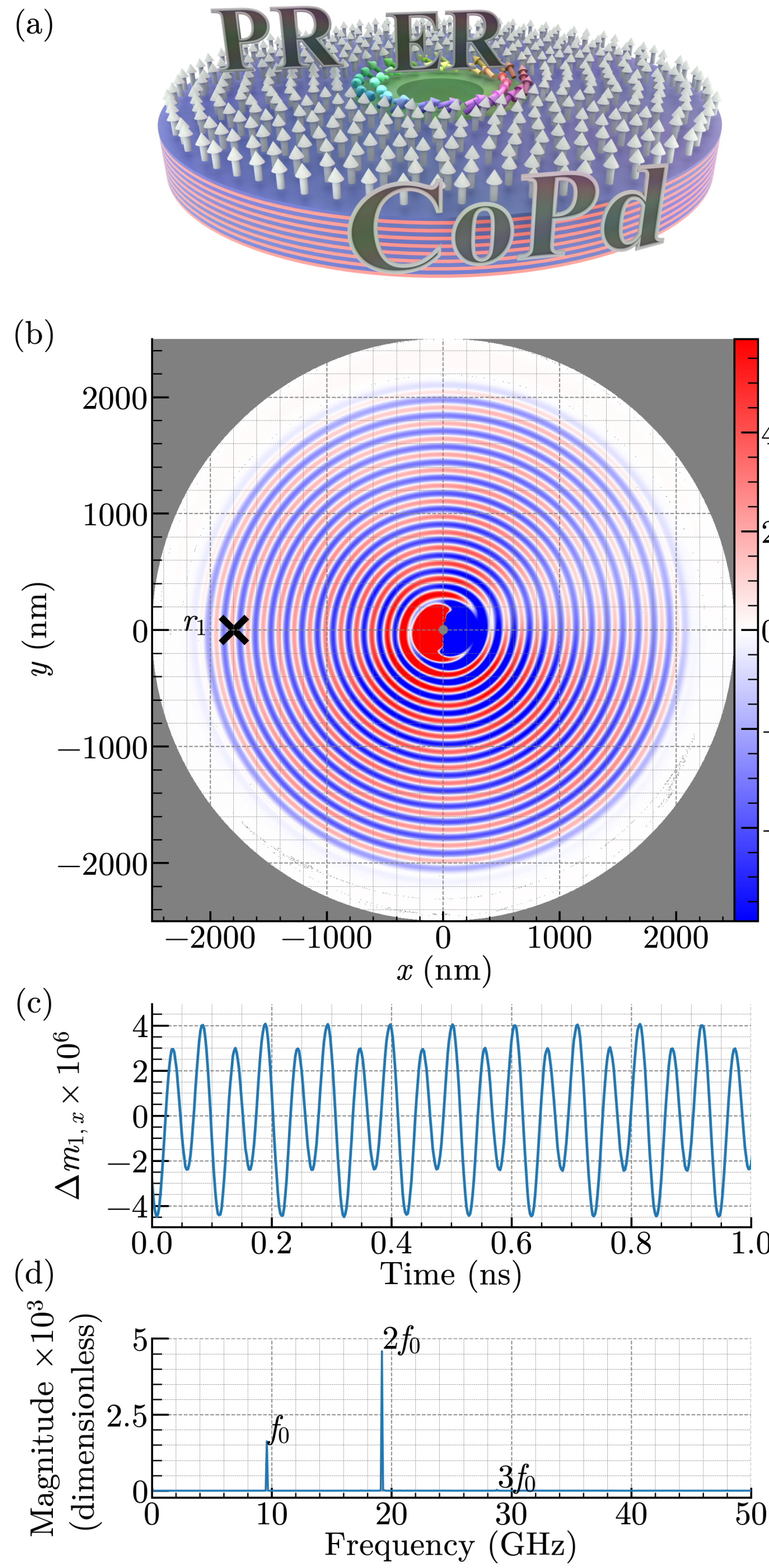
Mathieu Moalic*, Youenn Pata, Mateusz Zelent and Maciej Krawczyk

Institute of Spintronics and Quantum Information, Faculty of Physics and Astronomy, Adam Mickiewicz University, Poznań, Poland

* matmoa@amu.edu.pl

Spin waves (SWs) are attractive information carriers owing to their gigahertz–terahertz frequencies, nanometer-scale wavelengths, and negligible Joule heating. Yet, efficient excitation of *exchange-dominated* SWs, which intrinsically possess sub-300 nm wavelengths, remains challenging. We propose a hybrid nanostructure composed of an in-plane-magnetized rim exchange-coupled to an out-of-plane-magnetized Co/Pd strip. Micromagnetic simulations show that a spatially uniform, out-of-plane microwave field excites the rim’s fundamental mode whose *second harmonic* is coherently launched into the strip, yielding propagating SWs with wavelengths down to 260 nm. The conversion efficiency grows quasi-linearly with the pump amplitude, and the emission frequency is tunable via the bias field or rim width, suggesting a compact route toward on-chip short-wavelength SW sources.

2f₀ generation in a thin disk



We select a $[Co/Pd]_8$ multilayer (thickness 13.2 nm) with two regions of differing PMA: an Excitation Region (ER) lacking uniaxial anisotropy (in-plane at remanence) and a Propagation Region (PR) with strong PMA (fully out-of-plane at remanence), joined by a $\approx 90^\circ$ domain wall.

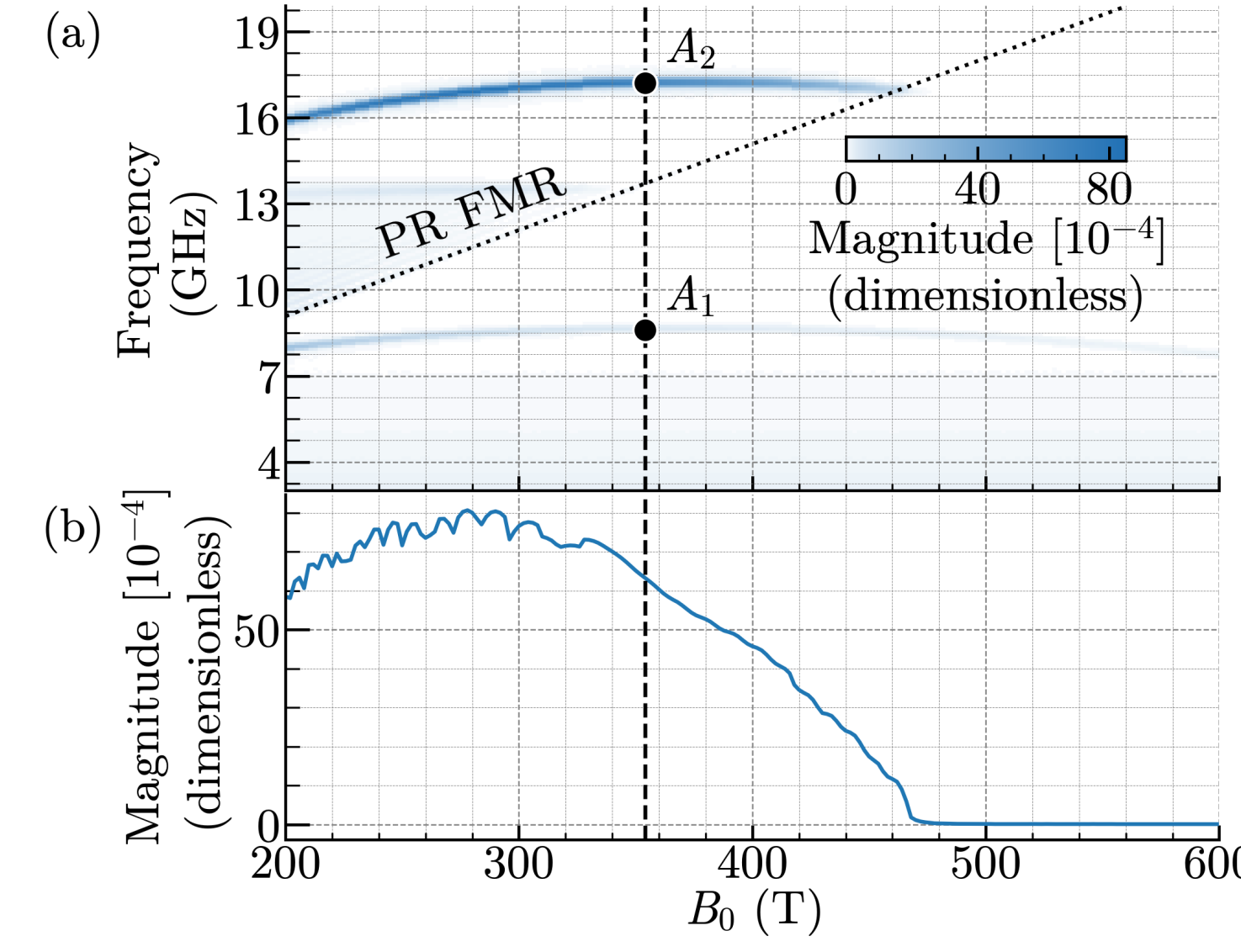
The results are obtained Amumax [1], a micromagnetic solver which is a for of MuMax3 [2]. The material parameters and the effective multilayer model are taken from Pan et al. [3].

Disk geometry: radius 2.5 μm with an 80 nm antidot and an ER rim of width $w = 40$ nm. A high-damping ring of width 500 nm near the outer edge suppresses reflections.

Broadband drive: a sinc pulse along z (cutoff ≈ 10 GHz, peak $b = 10$ mT) yields a single sub-cutoff peak at $f_0 = 8.61$ GHz. We then drive steadily at f_0 with $b = 100\ \mu T$, producing radially propagating SWs from the rim.

Spectral analysis at probe r_1 ($\approx 1.8\ \mu m$ from center) shows a dominant $2f_0$ component with weak f_0 and $3f_0$ signals.

Tuning 2f₀ by modulating the static field B_0



We vary the static field B_0 to tune the ER fundamental f_0 and its second harmonic. For each B_0 we re-compute f_0 , drive the system sinusoidally at f_0 with fixed amplitude $b = 100\ \mu T$, and record the PR response at $x = 2000$ nm.

The $2f_0$ branch tracks f_0 , rising from 16.0 to 17.25 GHz as B_0 increases from 200 to 354 mT, then bending downward and crossing the PR FMR at $B_z = 464$ mT (where $2f_0 = 16.5$ GHz).

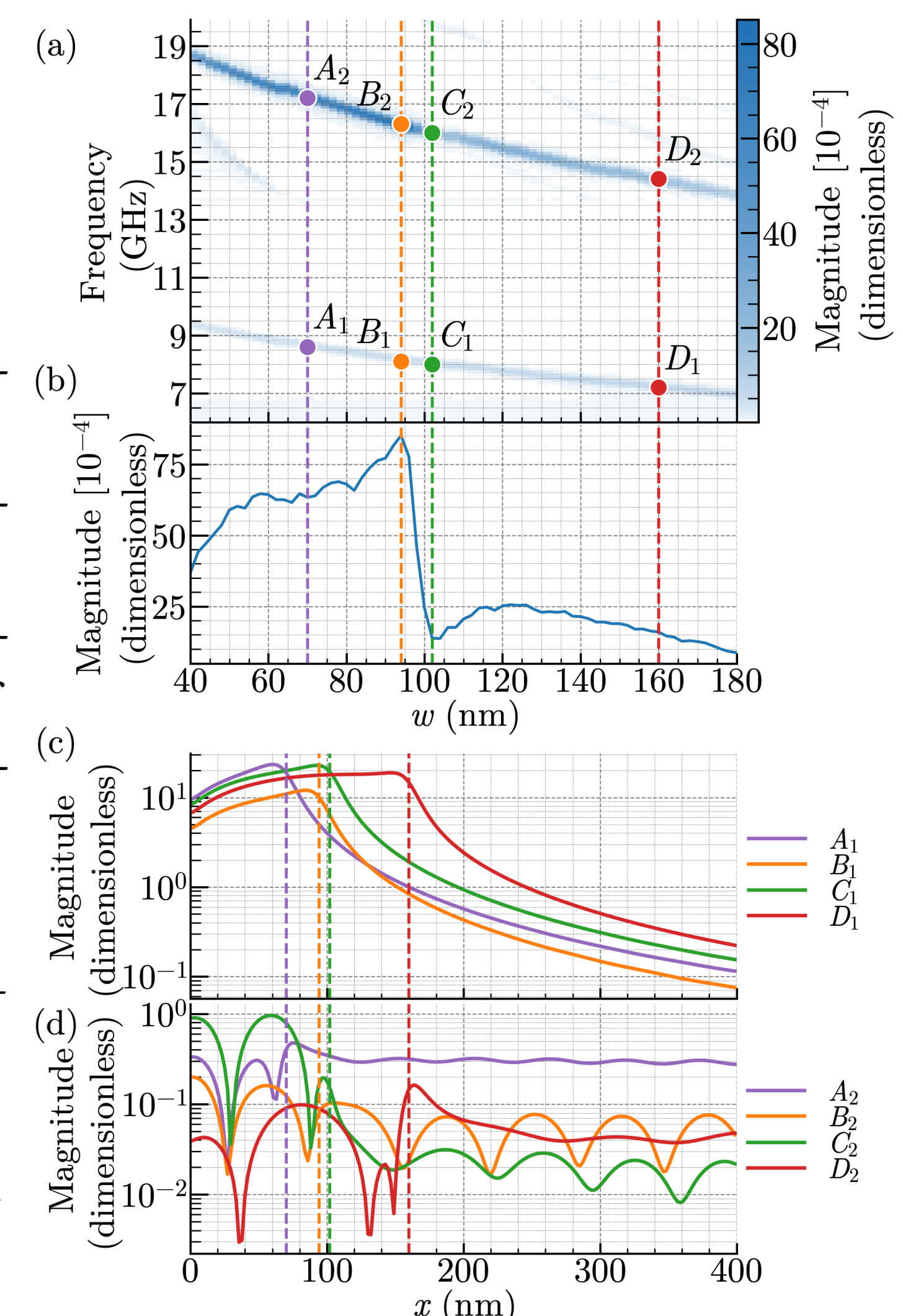
This strategy yields moderate $2f_0$ control—a 1.25 GHz span for a 160 mT change in B_0 —accompanied by concurrent changes in emitted intensity.

Tuning 2f₀ by modulating the excitation region width w

We set $B_z = 354$ mT and vary the ER width w from 30–180 nm (panel a). As w increases, f_0 decreases $8.60 \rightarrow 7.44$ GHz (so $2f_0$ shifts $17.20 \rightarrow 14.88$ GHz).

In panel b, we plot the $2f_0$ amplitude at $x = 2000$ nm as a function of w . The emission intensity grows with w , reaching a maximum at $w = 94$ nm, then dropping off. This is happening at the B_2 crossing point, where the $2f_0$ branch intersects a higher-order ER resonance at $w = 94$ nm. The spatial profiles of both branches perfectly match at the crossing point, creating a resonance that boosts the $2f_0$ emission intensity.

Fundamental f_0 modes— A_1, B_1, C_1, D_1 —share an invariant profile (panel c): tightly confined to the ER, peaking at the domain wall, and decaying evanescently into the PR (as f_0 lies below the PR cut-off). The $2f_0$ profiles (panel d) exhibit nodal points within the ER, as expected for higher harmonics: A_2, B_2, C_2 show two nodes, while D_2 shows three.



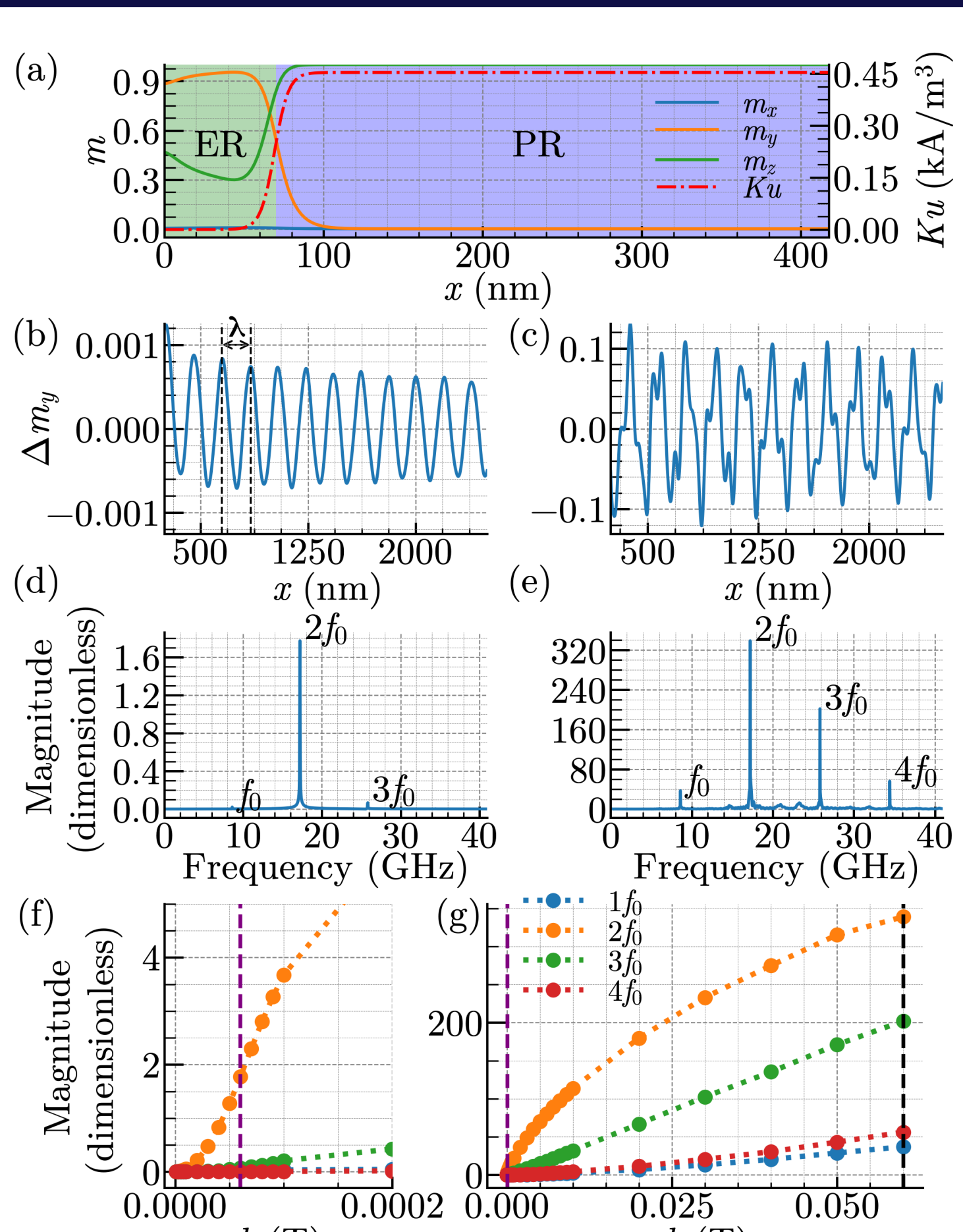
Conclusion

The presented mechanism of second-harmonic generation works in 1D/2D; the pumped fundamental f_0 is trapped in the ER while its second harmonic $2f_0$ propagates in the PR; the ER acts as a resonant nano-cavity that up-converts it to $2f_0$, efficiently launching into the PR. The second harmonic generation is significantly enhanced when at $2f_0$ a resonant condition for the standing wave formation in the ER is met. The emission frequency is tunable via B_0 or rim width w , efficiency scales linearly with pump. This offers a lithography-simple, energy-efficient source of exchange-dominated spin waves ($\lambda < 300$ nm) for magnonic logic, signal processing, and hybrid magnonic–quantum platforms.

One-Dimensional Case

To study the underlying phenomena more effectively, we reduce to a 1D geometry: length 3600 nm along x , a single simulation cell along y , and periodic boundary conditions (1000 unit-cell repetitions on each side). We run a steady-state drive at f_0 with $b = b_1 = 60\ \mu T$. Although f_0 lies below the PR FMR (13.90 GHz), a strong SW is observed in the PR, propagating along x with wavelength $\lambda = 261$ nm (panel b). A DFT of $m(x, t)$ at $x = 2\ \mu m$ (panel d) shows a pronounced $2f_0$ peak and only very weak components at f_0 and $3f_0$, consistent with the 2D result. Setting $b = b_2 = 60$ mT yields a richer waveform in the PR (panel c). The spectrum features a dominant $2f_0$ line and visible higher harmonics at $3f_0$ and $4f_0$ (panel e).

The $2f_0$ amplitude grows $\propto b^2$ up to $b \approx 0.1$ mT (panel f), then crosses over to $\propto \sqrt{b}$ (panels g), indicating additional processes become active near 0.1 mT. In this regime, the 3rd and 4th harmonics increase markedly, narrowing their gap to $2f_0$.



Bibliography

- [1] M. Moalic and M. Zelent, MathieuMoalic/amumax: 2023.10.26, (2023).
- [2] A. Vansteenkiste, J. Leliaert, M. Dvornik, M. Helsen, F. Garcia-Sanchez, and B. Van Waeyenberge, The design and verification of MuMax3, AIP Adv. **4**, 107133 (2014).
- [3] S. Pan, S. Mondal, M. Zelent, R. Szwierz, S. Pal, O. Hellwig, M. Krawczyk, and A. Barman, Edge localization of spin waves in antidot multilayers with perpendicular magnetic anisotropy, Phys. Rev. B **101**, 14403 (2020).